

Towards Accurate and Reliable Change Detection of Remote Sensing Images via Knowledge Review and Online Uncertainty Estimation

Zhenglai Li, Chang Tang, Xianju Li, Weiyang Xie, Kun Sun, Xinzhong Zhu

Abstract—Change detection (CD) is an essential task for various real-world applications, such as urban management and disaster assessment. However, previous methods primarily focus on improving the accuracy of CD, while neglecting the reliability of detection results. In this paper, we propose a novel change detection network, called AR-CDNet, which is able to provide accurate change maps and generate pixel-wise uncertainty. Specifically, an online uncertainty estimation branch is constructed to model the pixel-wise uncertainty, which is supervised by the difference between predicted change maps and corresponding ground truth during the training process. Furthermore, we introduce a knowledge review strategy to distill temporal change knowledge from low-level features to high-level ones, thereby enhancing the discriminability of temporal difference features. Finally, we aggregate the uncertainty-aware features extracted from the online uncertainty estimation branch with multi-level temporal difference features to improve the accuracy of CD. Once trained, our AR-CDNet can provide accurate change maps and evaluate pixel-wise uncertainty without ground truth. Experimental results on two benchmark datasets demonstrate the superior performance of AR-CDNet in the CD task. The demo code for our work will be publicly available at <https://github.com/guanyuezheng/AR-CDNet>.

Index Terms—Change detection, Knowledge review, Uncertainty estimation.

I. INTRODUCTION

Change detection (CD) aims to locate and segment the changes that are most relevant in the bi-temporal images captured at diverse periods in the same surface regions. As an important technique in remote sensing sense understanding, CD has received increased attention and been applied for many real-world applications, such as land-use change detecting [1], [2], urban management [3], [4], global resources monitoring [5], and damage assessment [6], [7].

Early conventional CD methods mainly rely on hand-crafted features [8], which significantly limit the detection accuracy for high-resolution and very high-resolution remote sensing

CD due to their low robustness and insufficient semantics. Recently, with the development of deep Convolutional Neural Networks (CNNs), deep learning has made significant progress in many computer vision tasks, such as semantic segmentation [9], [10], object detection [11], [12], and image retrieval [13]. Motivated by the powerful feature representation capability of CNNs, many deep learning-based CD approaches have been proposed and have achieved superior performance compared with traditional CD methods [14], [15].

Although previous research has made extensive efforts to improve the accuracy of CD results [14], high accuracy is not the only criterion for a robust CD model. In real-world applications, it is crucial to determine the confidence associated with the detection results so that users can make informed decisions. For instance, if a large number of predicted results have low confidence, users may disregard the results and select alternative CD methods for their tasks. Therefore, evaluating the trustworthiness of model in addition to detection accuracy is essential for CD methods. This issue motivates us to develop a trustworthy CD method that can not only provide accurate change results but also estimate pixel-wise uncertainty.

Based on the observations discussed above, we propose a novel change detection network, called AR-CDNet, which is designed to generate accurate change maps and estimate pixel-wise uncertainty by leveraging knowledge review and online uncertainty estimation, respectively. To measure uncertainty, we introduce an online uncertainty estimation branch, which dynamically estimates pixel-wise confidence and is supervised by the difference between predicted change maps and corresponding ground truth during training. To ensure accuracy, we design a knowledge review strategy that effectively captures the significant information of multi-level temporal difference features and avoids dilution of knowledge in a U-shape network. The knowledge review module employs two attention mechanisms, namely reverse attention and conflict attention, to review the knowledge among the multi-level temporal difference features. The reverse attention enables the network to refocus on the regions that are not segmented in the high-level features branch, while the conflict attention forces the network to pay more attention to the conflict regions between detection results from high-level and low-level features. This way, knowledge can be distilled from low-level features into high-level features, thereby improving the feature presentation capability of temporal difference features. Finally, the comprehensive knowledge of uncertainty-aware features captured from the online uncertainty estimation branch and multi-level

Manuscript received X XX, XXXX; revised X XX, XXXX. This work was supported in part by the National Science Foundation of China under Grant 62076228 and 62176242, and in part by Natural Science Foundation of Shandong Province under Grant ZR2021LZH001. (Corresponding author: Chang Tang.)

Z. Li, C. Tang, X. Li, and K. Sun are with the school of computer, China University of Geosciences, Wuhan, China. (E-mail: {yuezhenguan, tangchang, ddwhlxj, sunkun}@cug.edu.cn).

W. Xie is with the State Key Laboratory of Integrated Services Networks, Xidian University, Shaanxi, China. (E-mail: wzhang@xidian.edu.cn).

X. Zhu is with College of Mathematics, Physics and Information Engineering, Zhejiang Normal University, Jinhua, China, and also with the Research Institute of Ningbo Cixing Co. Ltd, Ningbo, China. (E-mail: zxz@zjnu.edu.cn).

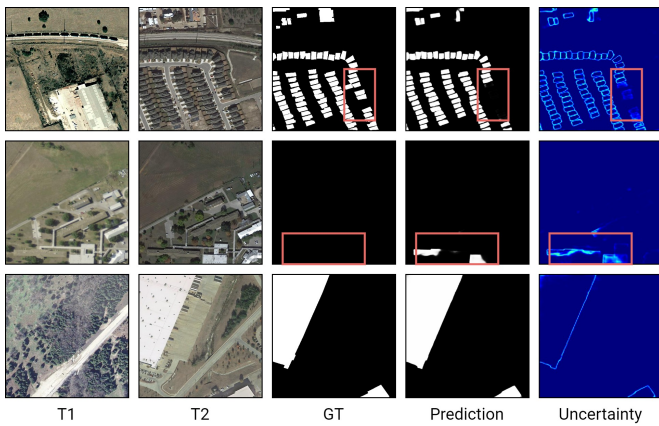


Fig. 1: Predictions of our AR-CDNet. From left to right: images at T1, T2, ground truth, predicated change maps, and uncertainty maps. The brighter regions indicate low confidence and dark blue regions denote high confidence. For hard sample shown in the first and second row, our predicated uncertainty map can effectively indicate the true-negative regions (highlighted with red box in first row) and false-positive regions (highlighted with red box in second row). For the easier sample shown in the third row, the estimated uncertainty mainly distribute along the boundary of changed objects.

temporal difference features are integrated for accurate change detection. Our results, as shown in Fig. 1, demonstrate that the predicted uncertainty map can assign true-negative regions and false-positive regions with lower confidence.

The main contributions of this work are summarized as follows:

- 1) We propose a novel change detection network, AR-CDNet, which can generate both accurate change maps and uncertainty maps by using knowledge review and online uncertainty estimation.
- 2) We introduce an online uncertainty estimation branch to model the pixel-wise uncertainty which is supervised by the difference between predicted change maps and ground truth in the training period. The uncertainty-aware features are further aggregated with multi-level temporal difference features to generate final change maps.
- 3) We propose a knowledge review module that includes reverse attention and conflict attention to effectively distill the temporal change knowledge of low-level features into high-level ones. Then, the multi-level temporal difference features are jointly explored to comprehensively identify changes.
- 4) We conduct a series of experiments on benchmark datasets to evaluate the effectiveness and superiority of our proposed AR-CDNet. Experimental results show that our approach outperforms various state-of-the-art models on two benchmark datasets.

This paper is organized as follows. Section II provides a brief review of related work in change detection. Section III presents the proposed method, including the network architecture, online uncertainty estimation branch, and knowledge

review module. In Section IV, extensive experiments are conducted on two benchmark datasets to evaluate the performance of the proposed AR-CDNet, with detailed discussions and model analyses. Finally, Section V concludes this paper.

II. RELATED WORK

A. Traditional CD Methods

Traditional change detection (CD) methods primarily employ image transformation [16], [17] and image algebra [18]–[22] techniques to identify changes in low- or middle-resolution remote sensing images. Previous methods typically utilize principal component analysis [16] and tasseled cap transformation [17] to enhance change information in bi-temporal images, thereby enabling easy detection of changes. Representative image algebra techniques-based methods, such as image difference [18], [23], image regression [19]–[22], and change vector analysis [24] are used to formulate difference images and choose suitable thresholds to identify changes. However, traditional CD methods rely on hand-crafted features that lack sufficient contextual information, resulting in limited performance for high-resolution and very high-resolution remote sensing CD.

B. Deep Learning-based CD Methods

Deep Learning-based CD Methods, with their powerful feature representation capability, have become the dominant solutions for high-resolution and very high-resolution remote sensing CD recently [14], [15], [25]–[36]. Previous methods boost the accuracy of CD mainly from the following aspects.

1) Multi-level feature fusion: As we know, the features extracted from the top layers of backbones are beneficial to locate objects, while that extracted from the bottom layers of backbones are conducive to recovering the details of objects [37]. In recent years, many works with various well-designed multi-level feature fusion architectures are proposed to boost CD performance [14], [15], [25]–[33]. For example, the long short-term memory (LSTM) and skip connection are combined to obtain more distinguishable multi-level features [38]. A full-scale feature fusion manner is introduced to aggregate multi-level information at diverse feature scales. Afterward, hybrid attention is utilized to capture the long-range context information among bi-temporal features for a more accurate CD. Li et al. [39] proposed a guided refinement model, which first aggregates multi-level features and then exploits the aggregated features to repetitively polish multi-level features, to filter out the irrelevant noise information mixed in multi-level features. More inspiring related works can refer to the recent survey [14].

2) Temporal difference extraction: Effectively capturing the temporal difference information from bi-temporal features also play a key component in CD. Previous methods usually employ feature concatenation or subtraction operations to realize temporal difference extraction. As demonstrated in [40], the original bi-temporal information can be preserved by the temporal concatenation operation, which stacks bi-temporal features along the dimension of channels in order. The feature subtraction needs an additional hand-crafted distance, e.g., ℓ_1

or ℓ_2 distance, to measure the pixel-wise temporal difference. Apart from the above two native temporal difference extraction manners, Zheng et al. [40] took the temporal order into consideration and designed a temporal-symmetric transformer, which exploits weight-shard 3-D convolutional layers with different temporal arrange orders to extract temporal difference information. Lei et al. [41] introduced a difference enhance module (DEM) based on the feature subtraction measure to select the most significant channels of bi-temporal features with a channel attention. Li et al. [39] considered the complementary aspects of feature concatenation or subtraction operation and designed a temporal feature interaction module, in which the change regions of bi-temporal features can be highlighted.

3) Attention mechanisms: In recent years, attention mechanisms have received intensive attention, due to their abilities in capturing the context information and boosting feature discriminability. Channel attention [42], convolution block attention module [43], and non-local [44] are three widely used attention mechanisms in the recently proposed CD method.

Previous methods have made significant efforts to improve the accuracy of CD but have overlooked the importance of confidence in their results. In real-world applications, it is crucial to provide confidence in detection results for users to make informed decisions in the absence of ground truth guidance. Therefore, solely pursuing detection accuracy while neglecting trustworthiness is inadequate for a robust CD method. This motivates us to propose a novel CD method that not only delivers accurate change results but also assesses pixel-wise uncertainty.

C. Uncertainty Estimation

Uncertainty estimation aims to formulate the uncertainty corresponding to the prediction of networks. In recent years, uncertainty estimation has progressively become an active research topic in some deep learning-based tasks, such as medical image segmentation [45], deep fake detection [46], hyperspectral image classification [47]. Two uncertainties, e.g., aleatoric uncertainty and epistemic uncertainty are widely studied in previous works [48], [49]. Aleatoric uncertainty tends to model the intrinsic randomness of the datasets resulting from the noise information during data collection, such as sensor noises. Epistemic uncertainty comes from the limited knowledge provided by the datasets. And epistemic uncertainty can be reduced with a larger and more diverse training dataset, giving a comprehensive understanding of the model. To model the aleatoric uncertainty, Shen et al, [50] introduced a teacher-student paradigm, in which multiple predictive samples are generated by the teacher network for the student network to learn with integrated aleatoric uncertainty. The Markov Chain Monte Carlo (MCMC) [51]–[53], variational inference [54], [55], and Ensemble-based methods [56] are three most representative strategies to approximate the epistemic uncertainty.

After uncertainty estimation, the obtained uncertainty maps can be further utilized to implement difficulty-aware learning [57], [58]. For example, Nie et al, [57] introduced a sample

selection strategy based on estimated confidence to force the network to pay more attention to hard samples. A pixel-adaptive convolution is filtered by the estimated confidence to strengthen the upsampling operation, which propagates pixels with high confidence into less reliable regions [58].

III. PROPOSED METHOD

In this section, the overview of the proposed AR-CDNet is first presented. Next, the structures of the online uncertainty estimation manner and knowledge review strategy are given in detail. Finally, we illustrate the loss function of AR-CDNet.

A. Overview

As shown in Fig. 2, we first utilize a shared feature extractor, which follows an encoder-decoder structure, to extract bi-temporal features. For the encoder, any backbone can be used here, and we utilize a ResNet18 [59] as done in previous methods [3], [39], [60] for a fair comparison. Let a registered pair of images be denoted as $\mathbf{I}^t \in \mathbb{R}^{h \times w \times 3}$, $t \in \{1, 2\}$, where h , w , and t denote the height, width and temporal order of images, respectively. Then, multi-level bi-temporal features, denoted as $\mathbf{F}_i^t \in \mathbb{R}^{h/2^{i+1} \times h/2^{i+1} \times c_i}$, $i \in \{2, 3, 4, 5\}$, $t \in \{1, 2\}$, can be obtained from the four stages of the encoder. The decoder is implemented in a U-shape structure, in which a feature aggregation module (FAM) is introduced to progressively fuse the multi-level context information from high-levels to low-levels. As shown in Fig. 3 (a), FAM first computes an element-wise weight from the high-level feature to calibrate the low-level feature, then high-level and low-level features are concatenated and pass through a convolution layer for feature fusion. With the decoder, we capture multi-level bi-temporal features $\mathbf{P}_i^t \in \mathbb{R}^{h/2^{i+1} \times h/2^{i+1} \times c_i}$, $i \in \{2, 3, 4, 5\}$, $t \in \{1, 2\}$ for detecting changes.

As discussed in the previous section, temporal difference extraction (TDE) is a key component of CD. Here, we adopt the temporal-symmetric transformer proposed in [40] (as shown in Fig. 3 (b)) to achieve TDE. The bi-temporal features are concatenated with two diverse temporal orders and pass through 3D convolution layers to capture temporal difference information. The procedure of TDE can be represented as,

$$\mathbf{D}_i = \mathcal{T}(\mathbf{P}_i^1, \mathbf{P}_i^2), i \in \{2, 3, 4, 5\}, \quad (1)$$

where $\mathcal{T}(\cdot)$ represents the function of TDE, \mathbf{D}_i denotes the obtained temporal difference features.

As illustrated previously, the U-shape structure progressively aggregates the multi-level information layer by layer. However, the long dependence between high-level and low-level features and the discriminative changed regions are ignored in such feature fusion strategy, resulting dilution of distinctive knowledge. To this end, the proposed knowledge review technique is exploited to fully capture the complementary information among multi-level temporal difference features for a more accurate CD. On the other hand, an online uncertainty estimation branch is designed to evaluate pixel-wise uncertainty of predicted change maps. From the online uncertainty estimation branch, the uncertainty-aware features are further combined with multi-level temporal difference

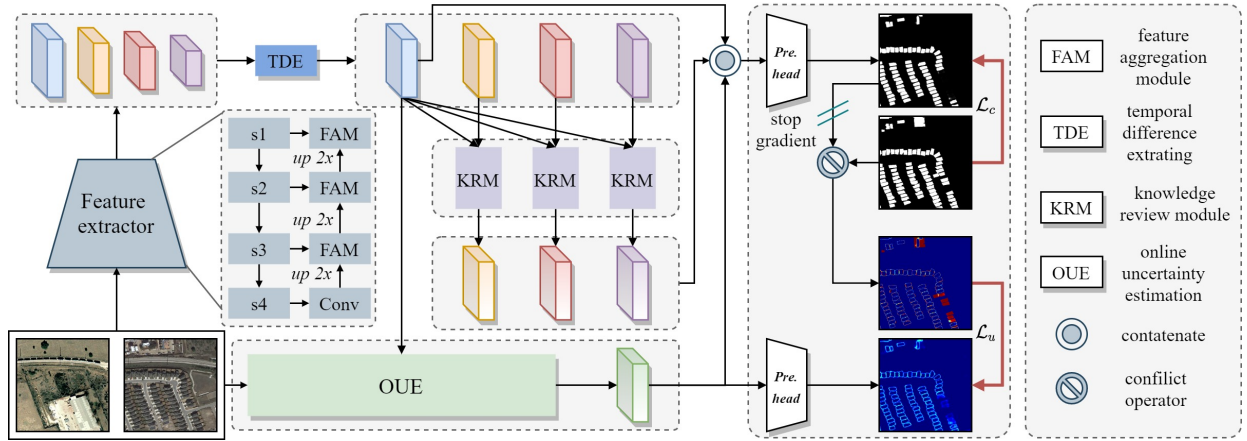


Fig. 2: A framework of the proposed AR-CDNet. Initially, the bi-temporal images pass through a shared feature extractor to obtain bi-temporal features, and then multi-level temporal difference features are obtained through the TDE. The OUE branch estimates pixel-wise uncertainty supervised by the diversity between predicted change maps and corresponding ground truth in the training process. KRMs fully explore the multi-level temporal difference knowledge. Finally, the multi-level temporal difference features and uncertainty-aware features obtained from the OUE branch are aggregated to generate the final change maps.

features to make the network pay more attention to the less reliable regions. More details of the knowledge review technique and online uncertainty estimation will be presented in Subsection III-C and III-B, respectively.

B. Online Uncertainty Estimation

The goal of uncertainty estimation is to determine the confidence related to the prediction of model on a pixel-wise basis. To achieve this, we introduce an online uncertainty estimation (OUE) branch, as shown in Figure 3 (c). OUE first uses three down-convolution blocks, implemented with three 3×3 convolutional layers, followed by batch normalization and ReLU functions, to extract texture information from the bi-temporal images. The temporal difference extracting (TDE) method is then employed to capture temporal difference information, which is further combined with the temporal difference features \mathbf{D}_2 via a FAM to capture comprehensive knowledge for uncertainty estimation. The entire process can be expressed as follows,

$$\begin{aligned} \mathbf{T}^t &= \text{DoB}(\mathbf{I}^t), t \in \{1, 2\}, \\ \mathbf{U} &= \mathcal{F}(\mathbf{D}_2, \mathcal{T}(\mathbf{T}^1, \mathbf{T}^2)), \end{aligned} \quad (2)$$

where $\text{DoB}(\cdot)$ and $\mathcal{F}(\cdot)$ denote the down-convolution blocks and FAM, respectively. \mathbf{T}^t and \mathbf{U} represent the bi-temporal texture features and uncertainty-aware features, respectively.

Intuitively, the network should have higher confidence in the true positive and false negative regions of the prediction but lower confidence in the false positive and false negative regions. Therefore, we aim to use the differences between the prediction of model and the corresponding ground truth as the supervision signal to guide the learning process of the OUE branch. The uncertainty supervision can be formulated as follows,

$$\mathbf{g}^u = \mathbf{p}^c \cdot (\mathbf{1} - \mathbf{g}^c) + \mathbf{g}^c \cdot (\mathbf{1} - \mathbf{p}^c), \quad (3)$$

where \mathbf{g}^u , \mathbf{p}^c , and \mathbf{g}^c represent the uncertainty supervision, predicted change map, and corresponding true changes, respectively. We train the OUE branch with a binary cross-entropy (BCE) loss \mathcal{L}_{bce} which is formulated as,

$$\mathcal{L}_u = \mathcal{L}_{bce}(\mathbf{p}^u, \mathbf{g}^u) = \mathbf{g}^u \cdot \log(\mathbf{p}^u) + (\mathbf{1} - \mathbf{g}^u) \cdot \log(\mathbf{1} - \mathbf{p}^u), \quad (4)$$

where \mathcal{L}_u denotes the uncertainty loss, \mathbf{p}_u is the predicted uncertainty map.

C. Knowledge Review

It is commonly acknowledged that the low-level features extracted from the bottom layers of the backbone contain abundant object details, while the high-level features obtained from the top layers of the backbone consist of semantic abstractions about the objects. To achieve accurate CD, it is crucial to fully utilize the information in both low-level and high-level features. Although the U-shaped structure of the feature extractor performs multi-level feature fusion, it fails to adequately explore the long dependence between high-level and low-level features and the discriminative changed regions, leading to the dilution of distinctive knowledge. To address this issue, we propose a knowledge review strategy consisting of three knowledge review modules (KRM). As illustrated in Fig. 4, a multi-branch structure equipped with conflict attention and reverse attention is utilized to capture the complementary information between the temporal difference features \mathbf{D}_2 and \mathbf{D}_3 .

As mentioned earlier, the multi-level temporal difference features capture diverse aspects of changed objects. To force the network to focus more on the conflicts between changed regions of high-level and low-level features and to extract the complementary information, we implement conflict attention. Let \mathbf{p}_2^c and \mathbf{p}_3^c denote the predicted change maps of temporal

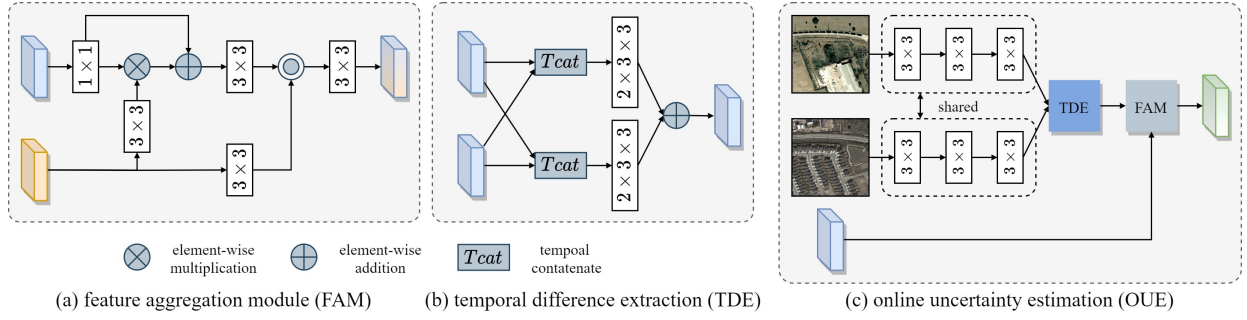


Fig. 3: Illustration of the feature aggregation module (FAM), temporal difference extracting (TDE), and online uncertainty estimation (OUE) branch.

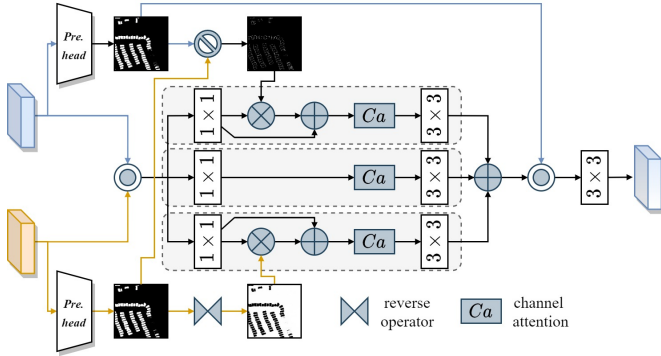


Fig. 4: Illustration of the knowledge review module (KRM).

difference features \mathbf{D}_2 and \mathbf{D}_3 , the conflicts regions can be calculated as the difference between \mathbf{p}_2^c and \mathbf{p}_3^c ,

$$\text{CoA} = \mathbf{p}_2^c \cdot (\mathbf{1} - \mathbf{p}_3^c) + \mathbf{p}_3^c \cdot (\mathbf{1} - \mathbf{p}_2^c), \quad (5)$$

where CoA is the obtained conflict attention between \mathbf{D}_2 and \mathbf{D}_3 .

In addition to conflict attention, we also introduce reverse attention to seek complementary information across multiple levels. High-level features are effective for object localization, but provide less detail about changed objects. Therefore, we exploit the low-level features to compensate for the insufficient detail in high-level features, guided by the reverse attention. Specifically, the reverse attention is formulated to erase the changed regions predicted by high-level features, thereby forcing the network to focus more on the unchanged regions. The reverse attention is formulated as,

$$\text{ReA} = (\mathbf{1} - \mathbf{p}_3^c), \quad (6)$$

where ReA denotes the reverse attention.

Afterwards, KRM concatenates \mathbf{D}_2 and \mathbf{D}_3 and pass through three 1×1 convolution layers for feature transition as,

$$\begin{aligned} \mathbf{D}_1^k &= \text{Conv}_{1 \times 1}(\text{Cat}(\mathbf{D}_2, \mathbf{D}_3)), \\ \mathbf{D}_2^k &= \text{Conv}_{1 \times 1}(\text{Cat}(\mathbf{D}_2, \mathbf{D}_3)), \\ \mathbf{D}_3^k &= \text{Conv}_{1 \times 1}(\text{Cat}(\mathbf{D}_2, \mathbf{D}_3)), \end{aligned} \quad (7)$$

where \mathbf{D}_1^k , \mathbf{D}_2^k , and \mathbf{D}_3^k denote the features for three branches of KRM. $\text{Cat}(\cdot)$ is the feature concatenate operator. The

conflict attention and reverse attention are plugged into two branches making the network capture the discriminative changed regions. In addition, a channel attention [42] subsequent with a 3×3 convolution layer is also injected into each branch of KRM for enhancing the feature representation capability. The whole process can be denoted as,

$$\begin{aligned} \mathbf{D}_1^r &= \text{Conv}_{3 \times 3}(\text{CA}(\mathbf{D}_1^k \oplus \mathbf{D}_1^k \otimes \text{CoA})), \\ \mathbf{D}_2^r &= \text{Conv}_{3 \times 3}(\text{CA}(\mathbf{D}_2^k \oplus \mathbf{D}_2^k \otimes \text{ReA})), \\ \mathbf{D}_3^r &= \text{Conv}_{3 \times 3}(\text{CA}(\mathbf{D}_3^k)), \end{aligned} \quad (8)$$

where \mathbf{D}_1^r , \mathbf{D}_2^r , \mathbf{D}_3^r are the enhanced features. $\text{CA}(\cdot)$, \oplus , and \otimes represent the channel attention, element-wise addition, and multiplication, respectively. Finally, \mathbf{D}_1^r , \mathbf{D}_2^r , \mathbf{D}_3^r and integrated into one representation, and further concatenate with the prediction \mathbf{p}_{2c} to generate final temporal difference features $\hat{\mathbf{D}}_3$ as,

$$\hat{\mathbf{D}}_3 = \text{Conv}_{3 \times 3}(\text{Cat}(\mathbf{p}_{2c}, \mathbf{D}_1^r \oplus \mathbf{D}_2^r \oplus \mathbf{D}_3^r)) \quad (9)$$

As shown in Fig. 2, three KRM are inserted in AR-CDNet to distill the fine-gained temporal change information into high-level features so as to fully capture the complementary information among multi-level temporal difference features. In this way, our AR-CDNet can provide more accurate change maps.

D. Loss Function

We jointly train the change detection part and online uncertainty estimation branch. For change detection part, a hybrid loss [39], [61] including a BCE loss \mathcal{L}_{bce} and a dice (Dice) loss \mathcal{L}_{dice} [62], is adopted as,

$$\mathcal{L}_c = \mathcal{L}_{bce} + \mathcal{L}_{dice} \quad (10)$$

where \mathcal{L}_c is the change detection loss.

With the uncertainty supervision, the total training loss of AR-CDNet can be formulated as,

$$\mathcal{L} = \mathcal{L}_c + \mathcal{L}_u \quad (11)$$

IV. EXPERIMENTS

A. Datasets

In our experiments, we use two remote sensing change detection benchmark datasets to evaluate the effectiveness of

TABLE I: Quantitative comparisons in terms of κ , IoU, F1, OA, Rec, and Pre on LEVIR+ and BCDD datasets. The best and second best results are highlighted in red and blue, respectively.

Datasets		FC-diff	FC-ef	FC-cat	L-UNet	DSIFN	SNUNet	BIT	MSCANet	TFI-GR	A2Net	Ours
Fps		124.30	178.31	122.76	28.93	15.60	14.42	44.85	53.78	77.23	56.48	28.85
FLOPs (G)		37.66	28.50	42.49	138.52	658.22	438.47	84.46	117.03	82.81	24.08	112.78
Params (M)		1.35	1.35	1.54	8.45	50.71	12.04	3.50	17.11	27.88	3.78	14.34
LEVIR+	κ	0.7148	0.5242	0.6346	0.7820	0.8386	0.7578	0.8175	0.8278	0.8074	0.8252	0.8582
	IoU	0.5705	0.3738	0.4822	0.6541	0.7318	0.6230	0.7016	0.7161	0.6884	0.7125	0.7605
	F1	0.7266	0.5442	0.6507	0.7909	0.8451	0.7677	0.8246	0.8346	0.8154	0.8321	0.8640
	Rec	0.7349	0.5617	0.7080	0.7918	0.8324	0.7736	0.7954	0.8124	0.8345	0.8127	0.8618
	Pre	0.7184	0.5277	0.6019	0.7899	0.8582	0.7619	0.8561	0.8580	0.7972	0.8525	0.8662
BCDD	κ	0.6103	0.4863	0.5037	0.6951	0.7312	0.6284	0.7019	0.6473	0.7449	0.7433	0.7683
	IoU	0.4544	0.3351	0.3507	0.5478	0.5896	0.4745	0.5555	0.4924	0.6078	0.6051	0.6370
	F1	0.6249	0.5020	0.5193	0.7079	0.7418	0.6436	0.7142	0.6599	0.7561	0.7539	0.7783
	Rec	0.5466	0.3866	0.4068	0.6816	0.6777	0.6065	0.6784	0.5590	0.7603	0.7217	0.7656
	Pre	0.7292	0.7158	0.7180	0.7363	0.8193	0.6856	0.7541	0.8052	0.7520	0.7892	0.7913

the proposed AR-CDNet. The detailed information is listed as follows,

LEVIR+ [63]: It is a expanded version of LEVIR [3], which consists of 637 pairs of bi-temporal remote sensing images captured from the Google Earth platform with 1024×1024 spatial size and 0.5m spatial resolution. LEVIR+ includes an additional 348 bi-temporal remote sensing images, with both datasets mainly focusing on building changes. In our experiments, we merge the validation and testing set of LEVIR to form a training set for LEVIR+. The additional 348 bi-temporal remote sensing images are used as a separate testing set. Due to limited GPU memory, all images are cropped into non-overlapping 512×512 patches. A total of 1780/768/1392 image pairs are obtained for training/validation/testing, respectively.

BCDD¹: It is a building change detection dataset containing a 32507×15354 bi-temporal images with 0.075m resolution. In our experiments, we none overlap crop the dataset into 512×512 size of patches and then obtained a total of 1827 pairs of bi-temporal images for the out-domain testing.

B. Evaluation Metrics

To verify the effectiveness of the proposed AR-CDNet, five widely used evaluation metrics [41], [64], [65], namely Kappa coefficient (κ), intersection over union (IoU), F1-score (F1), recall (Rec), and precision (Pre) are adopted in our experiments. The detailed calculations of five metrics can be found in [39], [61].

C. Implementation details

We implement the proposed AR-CDNet via the Pytorch toolbox [66]. Random flipping, cropping, and temporal exchanging are employed on the image patches for data augmentation. The AdamW [67] optimizer is exploited to optimize the proposed AR-CDNet, setting the weight decay and parameters β_1 , β_2 to 0.01, 0.9, and 0.99, respectively. We adopt the *poly* learning scheme to adjust the learning rate as $(1 - \frac{cur_iteration}{max_iteration})^{power} \times lr$, setting *power* and

max_iteration to 0.9 and 20000, respectively. The batch size is 8 and the initial learning rate is set as 0.0005. A single Nvidia Titan V GPU is used for training, validation, and testing.

D. Comparison With the State-of-the-art

We compare the proposed model with ten state-of-the-art remote sensing change detection approaches, including FC-Diff [68], FC-ef [68], FC-Cat [68], L-UNet [38], DSIFN [69], SNUNet [26], BIT [60], MSCANet [70], TFI-GR [39], and A2Net [61]. We reproduce the change detection results by using their released code under their default parameters for fair comparisons.

1) *Quantitative evaluation*: We present the quantitative evaluation results of various methods for remote sensing change detection, measured by κ , IoU, F1, Rec, and Pre, in Table I. In addition, Table I provides the FPS (Frames Per Second), model parameters (Params), and computation costs (FLOPs). The results show that the proposed AR-CDNet outperforms other methods in both in-domain and out-domain testing. For instance, on the LEVIR+ dataset (in-domain testing), the proposed AR-CDNet achieves approximately 1.96, 2.87, and 1.89 percentage higher performance improvements than the second-best method (DSIFN). On the BCDD dataset (out-domain testing), the proposed AR-CDNet achieves around 2.34, 2.92, and 2.22 percentage higher performance improvements than the second-best method (TFI-GR). Additionally, the proposed AR-CDNet has comparable FPS, model parameters, and computation costs to some heavy models, such as L-UNet, SNUNet, and DSIFN. These findings strongly demonstrate the effectiveness and superiority of the proposed AR-CDNet.

2) *Qualitative evaluation*: We present visual comparisons of various methods on LEVIR+ and BCDD datasets in Figs. 5 and 6, respectively. White, red, black, and blue are used to indicate true positives, false positives, true negatives, and false negatives, respectively, for better visualization. Based on the visual results in Figs. 5 and 6, we observe that the proposed method demonstrates superiority in the following aspects:

¹http://study.rsgis.whu.edu.cn/pages/download/building_dataset.html

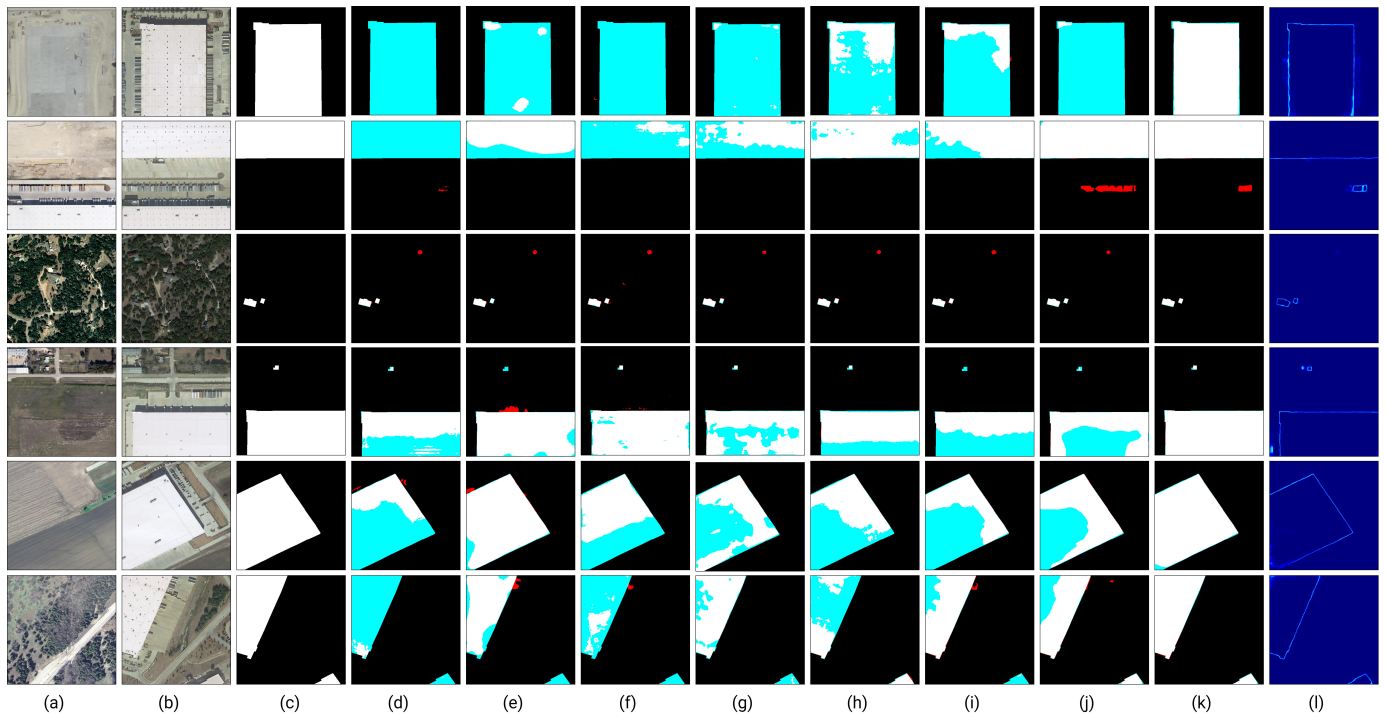


Fig. 5: Visual comparisons of the proposed method and the state-of-the-art approaches on the LEVIR+ dataset. (a) t_1 images; (b) t_2 images; (c) Ground-truth; (d) L-UNet; (e) DSIFN; (f) SNUNet; (g) BIT; (h) MSCANet; (i) TFI-GR; (j) A2Net; (k) Ours, (l) Predicted uncertainty map. The rendered colors represent true positives (white), false positives (red), true negatives (black), and false negatives (blue).

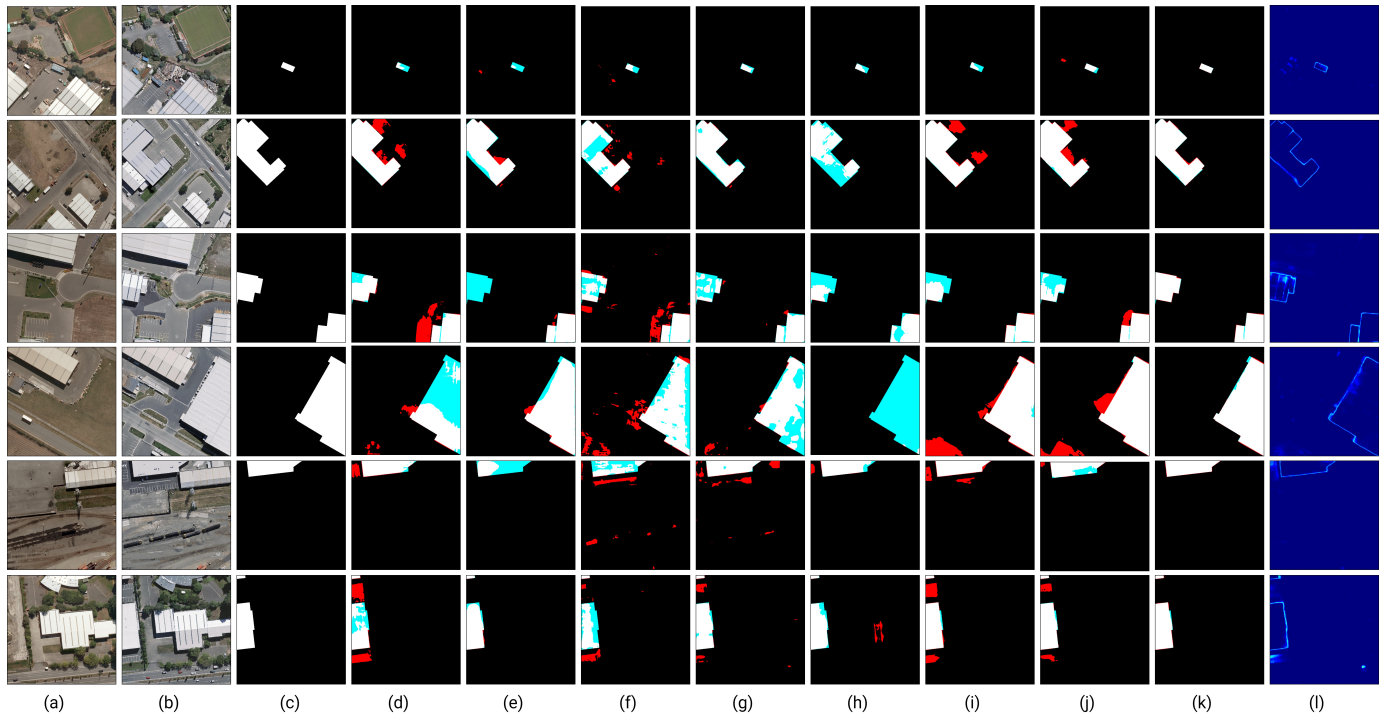


Fig. 6: Visual comparisons of the proposed method and the state-of-the-art approaches on the BCDD dataset. (a) t_1 images; (b) t_2 images; (c) Ground-truth; (d) L-UNet; (e) DSIFN; (f) SNUNet; (g) BIT; (h) MSCANet; (i) TFI-GR; (j) A2Net; (k) Ours, (l) Predicted uncertainty map. The rendered colors represent true positives (white), false positives (red), true negatives (black), and false negatives (blue).

- 1) *Advantages in Content Integrity*: In Fig. 5, it can be observed that some of the compared methods, such as L-Unet, DSIFN, SNUNet, BIT, MSCANet, TFI-GR, and A2Net, fail to detect the entire changed regions. On the other hand, the proposed AR-CDNet can accurately identify the changed objects with fine content integrity. The superior performance of our approach is attributed to two main reasons. Firstly, we employ a knowledge review approach to distill the fine-grained change information into coarse layers, and we jointly utilize the multi-level change information to comprehensively generate accurate change results. Secondly, our method estimates the uncertain regions, and we use a difficulty-aware learning approach to encourage the network to focus more on such uncertain regions, resulting in more precise change detection results.
- 2) *Advantages in Location Accuracy*: The visual results in Fig. 6 demonstrate that the proposed AR-CDNet accurately identifies the changed regions and effectively eliminates the irrelevant pseudo changes caused by background clutters in bi-temporal images. In contrast, several other methods, such as L-Unet, DSIFN, SNUNet, BIT, MSCANet, TFI-GR, and A2Net, fail to eliminate the irrelevant pseudo changes. These results underscore the efficacy of the proposed AR-CDNet.
- 3) *Advantages in Providing Accurate Uncertainty Maps*: The proposed AR-CDNet incorporates an uncertainty estimation approach to provide pixel-wise confidence levels associated with the predicted change maps. Our results in Figs. 5 and 6 indicate that the estimated uncertainty is mainly concentrated along the boundary of the changed objects, indicating high confidence when the predicted change maps are accurate. This highlights the effectiveness of the proposed uncertainty estimation approach.

E. Ablation Studies

We evaluate the effectiveness of the components and configurations of the proposed AR-CDNet on LEVIR+ and BCDD datasets and the diverse change detection performance measured by κ , IoU, F1, Rec, and Pre in Tab. II.

1) *Effectiveness of feature aggregation module (FAM)*: As demonstrated in the previous section, the Feature Aggregation Module (FAM) utilizes an element-wise weight calculated from high-level features to calibrate low-level features for better feature aggregation. To validate the effectiveness of FAM, we constructed an approach without the element-wise weight scheme and denoted it as FAM w/o G (#02 in TABLE II). The results in Tab. II show that when the element-wise weight scheme is removed, the change detection performance drops significantly. This indicates the effectiveness of the proposed FAM and emphasizes the importance of the element-wise weight scheme in achieving optimal performance.

2) *Effectiveness of online uncertainty estimation (OUE)*: In our proposed AR-CDNet, OUE is a key component for formulating the pixel-wise confidence related to the predicted change results and performing difficulty-aware region learning.

To verify its effectiveness, we first remove OUE module to set a w/o OUE method (#03 in TABLE II), of which the change detection performance is reported in TABLE II. As seen from the results, the change detection performance decreases respectively about 1.25, 1.67, and 1.23 percentages in terms of κ , IoU, and F1 on BCDD datasets. In addition, to demonstrating the effectiveness of difficulty-aware region learning in OUE, we only exploit the multi-level temporal difference features to obtain the final change detection, which is terms as OUE w/o UaL (#05 in TABLE II). We can observe that the difficulty-aware region learning manner can slightly improve the change detection performance, indicating its effectiveness.

To achieve OUE, we constructed a pseudo uncertainty supervision by modeling the difference between ground truth change maps and the final predicted change maps. To verify the effectiveness of the pseudo uncertainty supervision, we replaced it with the change boundary supervision and referred to this method as OUE w B sup (#04 in TABLE II). We observed that the pseudo uncertainty supervision obtained the best performance.

3) *Effectiveness of knowledge review module (KRM)*: We apply the KRM to distill the fine temporal change knowledge into high-level features and jointly use the multi-level temporal difference feature to generate the final change maps. The KRM consists of two key attention mechanisms: reverse attention and conflict attention. To validate the effectiveness of KRM, we formulate four variants of the proposed AR-CDNet, denoted as w/o KRM, KRM w/o CoA, KRM w/o ReA, and KRM w/o CoA & ReA, as #06-#09 in TABLE II. In w/o KRM, we remove the KRM and only use the initial multi-level temporal difference features and uncertainty-aware features to obtain the final change maps. For KRM w/o CoA and KRM w/o ReA, we separately remove the conflict attention and reverse attention. For KRM w/o CoA & ReA, we remove both the conflict attention and reverse attention from the network. From the results in TABLE II, we observe that using only the reverse attention or conflict attention has worse performance than the default setting. Therefore, the default setting of KRM, which uses both reverse attention and conflict attention, is the most effective choice.

F. Discussions about Failure Cases

Although the proposed AR-CDNet can achieve advancing change detection performance and provide pixel-wise uncertainty of the predicted change maps for the CD task in a global perspective, there are still some challenging cases that need to be addressed for further improvement. In Fig. 7, we present two representative failure cases from two remote sensing change detection datasets. In these cases, the proposed AR-CDNet predicts incorrect changed regions or fails to capture the entire changed regions due to the background clutters and changed objects exhibiting fewer differences from the background. Nonetheless, as discussed in IV-D1 and IV-D2, the improvements validate that the proposed AR-CDNet can effectively handle most challenging scenarios compared to state-of-the-art methods for CD tasks.

TABLE II: Quantitative comparisons of the proposed method with diverse settings in terms of κ , IoU, F1, OA, Rec, and Pre on LEVIR+ and BCDD datasets.

No.	Variants	LEVIR +					BCDD				
		κ	IoU	F1	Rec	Pre	κ	IoU	F1	Rec	Pre
#1	AR-CDNet	0.8582	0.7605	0.8640	0.8618	0.8662	0.7683	0.6370	0.7783	0.7656	0.7913
(a) Feature Aggregation Module (FAM)											
#2	FAM w/o Gate	0.8503	0.7488	0.8564	0.8458	0.8671	0.7445	0.6059	0.7546	0.6880	0.8353
(b) Online Uncertainty Estimation (OUE)											
#3	w/o OUE	0.8541	0.7543	0.8600	0.8485	0.8717	0.7558	0.6203	0.7656	0.7114	0.8288
#4	OUE w/o UaL	0.8556	0.7565	0.8614	0.8507	0.8724	0.7437	0.6043	0.7534	0.6672	0.8651
#5	OUE w B sup	0.8444	0.7402	0.8507	0.8431	0.8585	0.7487	0.6112	0.7587	0.6969	0.8325
(c) Knowledge Review Module (KRM)											
#6	w/o KRM	0.8209	0.7065	0.8280	0.8148	0.8417	0.7367	0.5960	0.7469	0.6749	0.8361
#7	KRM w/o CoA	0.8467	0.7436	0.8530	0.8579	0.8481	0.7771	0.6476	0.7861	0.7355	0.8442
#8	KRM w/o ReA	0.8478	0.7452	0.8540	0.8526	0.8553	0.7671	0.6352	0.7769	0.7491	0.8069
#9	KRM w/o ReA & CoA	0.8399	0.7336	0.8463	0.8384	0.8544	0.7474	0.6096	0.7575	0.6968	0.8297

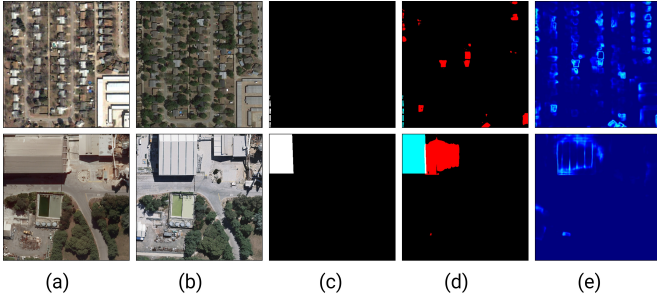


Fig. 7: Visual of some failure cases of the proposed AR-CDNet on two remote sensing change detection datasets. (a) t_1 images; (b) t_2 images; (c) Ground-truth; (d) Predicted change maps; (e) Evaluated uncertainty maps. The rendered colors represent true positives (white), false positives (red), true negatives (black), and false negatives (blue).

V. CONCLUSION

In this work, we introduce a novel change detection network that is capable of producing accurate and reliable change detection outcomes. The proposed method comprises a knowledge review module and an online uncertainty estimation branch, which respectively aim to achieve accurate and reliable change detection. The experimental results obtained on two high spatial resolution remote sensing change detection datasets demonstrate that the proposed approach outperforms state-of-the-art change detection methods.

ACKNOWLEDGMENT

The authors wish to gratefully acknowledge the anonymous reviewers for the constructive comments of this paper.

REFERENCES

[1] J. Deng, K. Wang, Y. Deng, and G. Qi, "Pca-based land-use change detection and analysis using multitemporal and multisensor satellite

data," *International Journal of Remote Sensing*, vol. 29, no. 16, pp. 4823–4838, 2008.

[2] Y. Hu, Y. Dong *et al.*, "An automatic approach for land-change detection and land updates based on integrated ndvi timing analysis and the cvaps method with gee support," *ISPRS Journal of Photogrammetry and Remote Sensing*, vol. 146, pp. 347–359, 2018.

[3] H. Chen and Z. Shi, "A spatial-temporal attention-based method and a new dataset for remote sensing image change detection," *Remote Sensing*, vol. 12, no. 10, p. 1662, 2020.

[4] H. Liu, M. Yang, J. Chen, J. Hou, and M. Deng, "Line-constrained shape feature for building change detection in vhr remote sensing imagery," *ISPRS International Journal of Geo-Information*, vol. 7, no. 10, p. 410, 2018.

[5] R. E. Kennedy, P. A. Townsend, J. E. Gross, W. B. Cohen, P. Bolstad, Y. Wang, and P. Adams, "Remote sensing change detection tools for natural resource managers: Understanding concepts and tradeoffs in the design of landscape monitoring projects," *Remote Sensing of Environment*, vol. 113, no. 7, pp. 1382–1396, 2009.

[6] F. Bovolo and L. Bruzzone, "A split-based approach to unsupervised change detection in large-size multitemporal images: Application to tsunami-damage assessment," *IEEE Transactions on Geoscience and Remote Sensing*, vol. 45, no. 6, pp. 1658–1670, 2007.

[7] Z. Zheng, Y. Zhong, J. Wang, A. Ma, and L. Zhang, "Building damage assessment for rapid disaster response with a deep object-based semantic change detection framework: From natural disasters to man-made disasters," *Remote Sensing of Environment*, vol. 265, p. 112636, 2021.

[8] Y. Sun, L. Lei, D. Guan, and G. Kuang, "Iterative robust graph for unsupervised change detection of heterogeneous remote sensing images," *IEEE Transactions on Image Processing*, vol. 30, pp. 6277–6291, 2021.

[9] Z. Jin, T. Gong, D. Yu, Q. Chu, J. Wang, C. Wang, and J. Shao, "Mining contextual information beyond image for semantic segmentation," in *International Conference on Computer Vision*, 2021, pp. 7231–7241.

[10] Z. Zheng, Y. Zhong, J. Wang, and A. Ma, "Foreground-aware relation network for geospatial object segmentation in high spatial resolution remote sensing imagery," in *Conference on Computer Vision and Pattern Recognition*, 2020, pp. 4096–4105.

[11] Y. Cui, L. Yan, Z. Cao, and D. Liu, "Tf-blender: Temporal feature blender for video object detection," in *International Conference on Computer Vision*, 2021, pp. 8138–8147.

[12] Z. Zheng, Y. Zhong, A. Ma, X. Han, J. Zhao, Y. Liu, and L. Zhang, "Hynet: Hyper-scale object detection network framework for multiple spatial resolution remote sensing imagery," *ISPRS Journal of Photogrammetry and Remote Sensing*, vol. 166, pp. 1–14, 2020.

[13] S. Kim, D. Kim, M. Cho, and S. Kwak, "Proxy anchor loss for deep metric learning," in *Conference on Computer Vision and Pattern Recognition*, 2020, pp. 3238–3247.

- [14] A. Shafique, G. Cao, Z. Khan, M. Asad, and M. Aslam, "Deep learning-based change detection in remote sensing images: a review," *Remote Sensing*, vol. 14, no. 4, p. 871, 2022.
- [15] L. Ru, B. Du, and C. Wu, "Multi-temporal scene classification and scene change detection with correlation based fusion," *IEEE Transactions on Image Processing*, vol. 30, pp. 1382–1394, 2020.
- [16] T. Celik, "Unsupervised change detection in satellite images using principal component analysis and k -means clustering," *IEEE Geoscience and Remote Sensing Letters*, vol. 6, no. 4, pp. 772–776, 2009.
- [17] E. P. Crist, "A tm tasseled cap equivalent transformation for reflectance factor data," *Remote Sensing of Environment*, vol. 17, no. 3, pp. 301–306, 1985.
- [18] L. Bruzzone and D. F. Prieto, "Automatic analysis of the difference image for unsupervised change detection," *IEEE Transactions on Geoscience and Remote Sensing*, vol. 38, no. 3, pp. 1171–1182, 2000.
- [19] P. R. Coppin and M. E. Bauer, "Digital change detection in forest ecosystems with remote sensing imagery," *Remote Sensing Reviews*, vol. 13, no. 3–4, pp. 207–234, 1996.
- [20] Y. Sun, L. Lei, X. Tan, D. Guan, J. Wu, and G. Kuang, "Structured graph based image regression for unsupervised multimodal change detection," *ISPRS Journal of Photogrammetry and Remote Sensing*, vol. 185, pp. 16–31, 2022.
- [21] Y. Sun, L. Lei, D. Guan, M. Li, and G. Kuang, "Sparse-constrained adaptive structure consistency-based unsupervised image regression for heterogeneous remote-sensing change detection," *IEEE Transactions on Geoscience and Remote Sensing*, vol. 60, pp. 1–14, 2022.
- [22] Y. Sun, L. Lei, X. Li, X. Tan, and G. Kuang, "Structure consistency-based graph for unsupervised change detection with homogeneous and heterogeneous remote sensing images," *IEEE Transactions on Geoscience and Remote Sensing*, vol. 60, pp. 1–21, 2022.
- [23] W. Zhang, L. Jiao, F. Liu, S. Yang, and J. Liu, "Adaptive contourlet fusion clustering for sar image change detection," *IEEE Transactions on Image Processing*, vol. 31, pp. 2295–2308, 2022.
- [24] E. F. Lambin and A. H. Strahlers, "Change-vector analysis in multitemporal space: A tool to detect and categorize land-cover change processes using high temporal-resolution satellite data," *Remote Sensing of Environment*, vol. 48, no. 2, pp. 231–244, 1994.
- [25] D. Peng, Y. Zhang, and H. Guan, "End-to-end change detection for high resolution satellite images using improved unet++," *Remote Sensing*, vol. 11, no. 11, p. 1382, 2019.
- [26] S. Fang, K. Li, J. Shao, and Z. Li, "Snunet-cd: A densely connected siamese network for change detection of vhr images," *IEEE Geoscience and Remote Sensing Letters*, vol. 19, pp. 1–5, 2022.
- [27] Z. Zheng, A. Ma, L. Zhang, and Y. Zhong, "Change is everywhere: Single-temporal supervised object change detection in remote sensing imagery," in *International Conference on Computer Vision*, 2021, pp. 15 193–15 202.
- [28] Y. Zhan, K. Fu, M. Yan, X. Sun, H. Wang, and X. Qiu, "Change detection based on deep siamese convolutional network for optical aerial images," *IEEE Geoscience and Remote Sensing Letters*, vol. 14, no. 10, pp. 1845–1849, 2017.
- [29] M. Zhang, G. Xu, K. Chen, M. Yan, and X. Sun, "Triplet-based semantic relation learning for aerial remote sensing image change detection," *IEEE Geoscience and Remote Sensing Letters*, vol. 16, no. 2, pp. 266–270, 2018.
- [30] J. Liu, M. Gong, K. Qin, and P. Zhang, "A deep convolutional coupling network for change detection based on heterogeneous optical and radar images," *IEEE Transactions on Neural Networks and Learning Systems*, vol. 29, no. 3, pp. 545–559, 2016.
- [31] M. Wang, K. Tan, X. Jia, X. Wang, and Y. Chen, "A deep siamese network with hybrid convolutional feature extraction module for change detection based on multi-sensor remote sensing images," *Remote Sensing*, vol. 12, no. 2, p. 205, 2020.
- [32] W. Zhao, L. Mou, J. Chen, Y. Bo, and W. J. Emery, "Incorporating metric learning and adversarial network for seasonal invariant change detection," *IEEE Transactions on Geoscience and Remote Sensing*, vol. 58, no. 4, pp. 2720–2731, 2019.
- [33] X. Tang, H. Zhang, L. Mou, F. Liu, X. Zhang, X. X. Zhu, and L. Jiao, "An unsupervised remote sensing change detection method based on multiscale graph convolutional network and metric learning," *IEEE Transactions on Geoscience and Remote Sensing*, vol. 60, pp. 1–15, 2022.
- [34] M. Lin, G. Yang, and H. Zhang, "Transition is a process: Pair-to-video change detection networks for very high resolution remote sensing images," *IEEE Transactions on Image Processing*, vol. 32, pp. 57–71, 2022.
- [35] M. Hu, C. Wu, B. Du, and L. Zhang, "Binary change guided hyperspectral multiclass change detection," *IEEE Transactions on Image Processing*, 2023.
- [36] Y. Lei, D. Peng, P. Zhang, Q. Ke, and H. Li, "Hierarchical paired channel fusion network for street scene change detection," *IEEE Transactions on Image Processing*, vol. 30, pp. 55–67, 2020.
- [37] T.-Y. Lin, P. Dollár, R. Girshick, K. He, B. Hariharan, and S. Belongie, "Feature pyramid networks for object detection," in *IEEE Conference on Computer Vision and Pattern Recognition*, 2017, pp. 2117–2125.
- [38] M. Papadomanolaki, M. Vakalopoulou, and K. Karantzalos, "A deep multitask learning framework coupling semantic segmentation and fully convolutional lstm networks for urban change detection," *IEEE Transactions on Geoscience and Remote Sensing*, vol. 59, no. 9, pp. 7651–7668, 2021.
- [39] Z. Li, C. Tang, L. Wang, and A. Y. Zomaya, "Remote sensing change detection via temporal feature interaction and guided refinement," *IEEE Transactions on Geoscience and Remote Sensing*, vol. 60, pp. 1–11, 2022.
- [40] Z. Zheng, Y. Zhong, S. Tian, A. Ma, and L. Zhang, "Changemask: Deep multi-task encoder-transformer-decoder architecture for semantic change detection," *ISPRS Journal of Photogrammetry and Remote Sensing*, vol. 183, pp. 228–239, 2022.
- [41] T. Lei, J. Wang, H. Ning, X. Wang, D. Xue, Q. Wang, and A. K. Nandi, "Difference enhancement and spatial-spectral nonlocal network for change detection in vhr remote sensing images," *IEEE Transactions on Geoscience and Remote Sensing*, vol. 60, pp. 1–13, 2022.
- [42] J. Hu, L. Shen, and G. Sun, "Squeeze-and-excitation networks," in *IEEE Conference on Computer Vision and Pattern Recognition*, 2018, pp. 7132–7141.
- [43] S. Woo, J. Park, J.-Y. Lee, and I. S. Kweon, "Cbam: Convolutional block attention module," in *European Conference on Computer Vision*, 2018, pp. 3–19.
- [44] X. Wang, R. Girshick, A. Gupta, and K. He, "Non-local neural networks," in *IEEE Conference on Computer Vision and Pattern Recognition*, 2018, pp. 7794–7803.
- [45] A. Mehrtash, W. M. Wells, C. M. Tempany, P. Abolmaesumi, and T. Kapur, "Confidence calibration and predictive uncertainty estimation for deep medical image segmentation," *IEEE transactions on medical imaging*, vol. 39, no. 12, pp. 3868–3878, 2020.
- [46] L. Trinh, M. Tsang, S. Rambhatla, and Y. Liu, "Interpretable and trustworthy deepfake detection via dynamic prototypes," in *IEEE Winter Conference on Applications of Computer Vision*, 2021, pp. 1973–1983.
- [47] X. He, Y. Chen, and L. Huang, "Toward a trustworthy classifier with deep cnn: Uncertainty estimation meets hyperspectral image," *IEEE Transactions on Geoscience and Remote Sensing*, vol. 60, pp. 1–15, 2022.
- [48] L. Kong, J. Sun, and C. Zhang, "Sde-net: equipping deep neural networks with uncertainty estimates," in *International Conference on Machine Learning*, 2020, pp. 5405–5415.
- [49] J. Zhang, Y. Dai, M. Xiang, D.-P. Fan, P. Moghadam, M. He, C. Walder, K. Zhang, M. Harandi, and N. Barnes, "Dense uncertainty estimation," *arXiv preprint arXiv:2110.06427*, 2021.
- [50] Y. Shen, Z. Zhang, M. R. Sabuncu, and L. Sun, "Real-time uncertainty estimation in computer vision via uncertainty-aware distribution distillation," in *IEEE Winter Conference on Applications of Computer Vision*, 2021, pp. 707–716.
- [51] R. M. Neal, *Bayesian learning for neural networks*. Springer Science & Business Media, 2012, vol. 118.
- [52] M. Welling and Y. W. Teh, "Bayesian learning via stochastic gradient langevin dynamics," in *International Conference on Machine Learning*, 2011, pp. 681–688.
- [53] W. Gong, Y. Li, and J. M. Hernández-Lobato, "Meta-learning for stochastic gradient MCMC," in *International Conference on Learning Representations*, 2019. [Online]. Available: <https://openreview.net/forum?id=HkeoOo09YX>
- [54] A. Wu, S. Nowozin, E. Meeds, R. E. Turner, J. M. Hernandez-Lobato, and A. L. Gaunt, "Deterministic variational inference for robust bayesian neural networks," in *International Conference on Learning Representations*, 2019. [Online]. Available: <https://openreview.net/forum?id=B1108oAct7>
- [55] C. Louizos and M. Welling, "Multiplicative normalizing flows for variational bayesian neural networks," in *International Conference on Machine Learning*, 2017, pp. 2218–2227.
- [56] B. Lakshminarayanan, A. Pritzel, and C. Blundell, "Simple and scalable predictive uncertainty estimation using deep ensembles," *Advances in Neural Information Processing Systems*, vol. 30, 2017.

- [57] D. Nie, L. Wang, L. Xiang, S. Zhou, E. Adeli, and D. Shen, "Difficulty-aware attention network with confidence learning for medical image segmentation," in *AAAI Conference on Artificial Intelligence*, vol. 33, no. 01, 2019, pp. 1085–1092.
- [58] A. S. Wannenwetsch and S. Roth, "Probabilistic pixel-adaptive refinement networks," in *IEEE Conference on Computer Vision and Pattern Recognition*, 2020, pp. 11 642–11 651.
- [59] K. He, X. Zhang, S. Ren, and J. Sun, "Deep residual learning for image recognition," in *IEEE Conference on Computer Vision and Pattern Recognition*, 2016, pp. 770–778.
- [60] H. Chen, Z. Qi, and Z. Shi, "Remote sensing image change detection with transformers," *IEEE Transactions on Geoscience and Remote Sensing*, vol. 60, pp. 1–14, 2022.
- [61] Z. Li, C. Tang, X. Liu, W. Zhang, J. Dou, L. Wang, and A. Y. Zomaya, "Lightweight remote sensing change detection with progressive feature aggregation and supervised attention," *IEEE Transactions on Geoscience and Remote Sensing*, vol. 61, pp. 1–12, 2023.
- [62] F. Milletari, N. Navab, and S.-A. Ahmadi, "V-net: Fully convolutional neural networks for volumetric medical image segmentation," in *International Conference on 3D Vision*, 2016, pp. 565–571.
- [63] L. Shen, Y. Lu, H. Chen, H. Wei, D. Xie, J. Yue, R. Chen, S. Lv, and B. Jiang, "S2looking: A satellite side-looking dataset for building change detection," *Remote Sensing*, vol. 13, no. 24, p. 5094, 2021.
- [64] L. Ding, H. Guo, S. Liu, L. Mou, J. Zhang, and L. Bruzzone, "Bi-temporal semantic reasoning for the semantic change detection in hr remote sensing images," *IEEE Transactions on Geoscience and Remote Sensing*, vol. 60, pp. 1–14, 2022.
- [65] J. Huang, Q. Shen, M. Wang, and M. Yang, "Multiple attention siamese network for high-resolution image change detection," *IEEE Transactions on Geoscience and Remote Sensing*, vol. 60, pp. 1–16, 2022.
- [66] A. Paszke, S. Gross, F. Massa, A. Lerer, J. Bradbury, G. Chanan, T. Killeen, Z. Lin, N. Gimeshein, L. Antiga *et al.*, "Pytorch: An imperative style, high-performance deep learning library," *Advances in Neural Information Processing Systems*, vol. 32, 2019.
- [67] I. Loshchilov and F. Hutter, "Decoupled weight decay regularization," in *International Conference on Learning Representations*, 2017.
- [68] R. C. Daudt, B. Le Saux, and A. Boulch, "Fully convolutional siamese networks for change detection," in *International Conference on Image Processing*, 2018, pp. 4063–4067.
- [69] C. Zhang, P. Yue, D. Tapete, L. Jiang, B. Shangguan, L. Huang, and G. Liu, "A deeply supervised image fusion network for change detection in high resolution bi-temporal remote sensing images," *ISPRS Journal of Photogrammetry and Remote Sensing*, vol. 166, pp. 183–200, 2020.
- [70] M. Liu, Z. Chai, H. Deng, and R. Liu, "A cnn-transformer network with multiscale context aggregation for fine-grained cropland change detection," *IEEE Journal of Selected Topics in Applied Earth Observations and Remote Sensing*, vol. 15, pp. 4297–4306, 2022.